

UC Berkeley

UC Berkeley Previously Published Works

Title

Field-induced heterophase state in PbZrO₃ thin films

Permalink

<https://escholarship.org/uc/item/7403d7q2>

Journal

Physical Review B, 105(12)

ISSN

2469-9950

Authors

Burkovsky, Roman G
Lityagin, Georgiy A
Ganzha, Alexander E
et al.


Publication Date

2022-03-01

DOI

10.1103/physrevb.105.125409

Peer reviewed

Field-induced heterophase state in PbZrO₃ thin filmsRoman G. Burkovsky,^{1,*} Georgiy A. Lityagin¹, Alexander E. Ganzha¹, Alexander F. Vakulenko,¹ Ran Gao,² Arvind Dasgupta,² Bin Xu³, Alexey V. Filimonov^{1,4} and Lane W. Martin^{2,5}¹*Peter the Great Saint-Petersburg Polytechnic University, 29 Politekhnicheskaya, 195251, St. Petersburg, Russia*²*Department of Materials Science and Engineering, University of California, Berkeley, California 94720, USA*³*School of Physical Science and Technology, Soochow University, Suzhou 215006, China*⁴*Alferov University, 8-3-A Khlopina, 194021, St. Petersburg, Russia*⁵*Materials Sciences Division, Lawrence Berkeley National Laboratory, Berkeley, California 94720, USA* (Received 13 January 2021; revised 22 February 2022; accepted 23 February 2022; published 11 March 2022)

Applications of epitaxial antiferroelectrics face scientific challenges, such as limited understanding of degraded (in comparison to bulk) switching behavior and its relation to nanoscale structural organization. We report on an unusual structural response of PbZrO₃/SrRuO₃/SrTiO₃ (001) heterostructures to precritical (lower than required for switching) electric fields. *In situ* x-ray diffraction shows a ferrielectric-like structure, which forms gradually upon increasing the applied field and makes up a heterophase state with the host antiferroelectric phase. The field-induced structure is similar to the antiferroelectric parent phase in the octahedral-tilt pattern, but differs from it in the lead-ion displacement pattern. The latter can be encoded as ↑↑↑↑ ↓↑↑↓ provided that the antiferroelectric structure is encoded as ↓↓↑↑. We propose that the unusual commensuratness (as opposed to the more ubiquitous incommensuration in similar materials) between the modulation periods of host and guest phases can be explained by accounting for the energy of heterophase boundaries, which is important in dense nanostructures due to the high surface-to-bulk ratio of nanodomains. An analysis using the *ab-initio*-correlated, but empirical (parametrized) energy model suggests that the observed field-induced structure is likely to be selected in PbZrO₃ instead of the others in the case when the above commensuration effect is at play. The results point to the mechanism leading to the smearing of polarization-field loops in such heterostructures and suggest a perspective for the controlled creation of delicate dipolar orderings for ferroic-based memory.

DOI: [10.1103/PhysRevB.105.125409](https://doi.org/10.1103/PhysRevB.105.125409)**I. INTRODUCTION**

Ferroelectric (FE) epitaxial thin films have attracted intense research interest [1–3]. Atom-to-atom correspondence between the film and substrate offers the possibility of building high-quality and defect-free heterostructures for miniaturized devices and also allows tailoring of the material properties by a set of size effects specific to films [4]. Although these size effects often limit the potential device performance [5,6], some of their combinations can also lead to exceptionally unusual polarization structures, such as vortices [7] and skyrmions [8] in epitaxial superlattices. A better understanding of those specifics is expected to reveal a rich set of interesting and practically useful phenomena.

Antiferroelectric (AFE) films are, as yet, much less studied than ferroelectric films and there is no solid theoretical basis for understanding them. These materials are, nevertheless interesting due to prospective applications in memory [9,10], energy storage [11–13], and electrocaloric devices [14,15]. Epitaxial films of the prototypical antiferroelectric, PbZrO₃, on SrRuO₃ conductive electrode, which is, in turn, deposited on ABO₃ perovskite substrate with large lattice mismatch (about 5%) compared to the PbZrO₃, are among the most thoroughly studied samples of this sort [16–19].

The strain in these films is quickly relaxed via dislocations in the near-interface layer [18]. Experimentally, the properties of PbZrO₃/SrRuO₃/SrTiO₃ heterostructures are substantially different from those of bulk PbZrO₃, namely ferroelectric islands were reported in the near-interface layer, which can occupy the entire film volume if the film is sufficiently thin [18]. Simultaneously, these heterostructures show a modified behavior with respect to switching between the antiferroelectric and the field-induced polar structures by electric field. As compared to the case of thicker polycrystalline films [20,21], where polarization-field (*P-E*) curves are notably linear between the points of field-induced transitions, thin epitaxial films show a more smeared *P-E* response. The *P-E* loops open and a remnant polarization appears at zero field [17–19]. In some experiments, the authors observed a smaller single ferroelectric-like loop inside the antiferroelectric double loop [17], while in other experiments no such loop was registered [18,19].

This film-specific antiferroelectric behavior has not yet been analyzed with the same rigor as has been done for ferroelectric thin films (see Refs. [4,22] for reviews); the existing interpretation is rather qualitative. The stabilization of the near-interface polar phase has been attributed to the effect of epitaxial strain [18]. This is compatible with the *ab initio* predictions of Reyes-Lillo and Rabe [23], who suggested that a compressive strain should stabilize the rhombohedral-like (or more likely monoclinic, due to strain)

*roman.burkovsky@gmail.com

ferroelectric phase. When a small ferroelectric-like P - E loop exists inside a double loop [17], this can be tentatively associated with the switching of a ferroelectric near-interface layer. When no such loop is visible [18,19], the interpretation is less clear because the modified layer can still be observed by electron microscopy [18], but its switching cannot be straightforwardly distinguished. Insight into this discrepancy can be obtained by considering the so-called *static* hysteresis loops of Ref. [18], which are measured with an alternative approach to the current integration in the hope of better reliability of the results. In the static regime, the P - E curve ceases to be open at zero field and attains an apparently linear section that spans between the field values where AFE-to-FE switching occurs. Although such a linear section is expected in a totally normal antiferroelectric case [22], the slope of this section (about 4.4 nF/m) is unusually high. It corresponds to the effective dielectric constant of about 500, which is more than two times larger than the dielectric constant value of 200 extracted from small-signal dielectric measurements at room temperature [19]. Such a discrepancy is usually not observed in thicker polycrystalline films, where the small-signal dielectric constant and the dielectric constant extracted from loops are quantitatively similar [20,21]. The unusually high effective dielectric constant extracted from the P - E loops of epitaxial PbZrO_3 could come from extrinsic contributions, such as field-induced movement of domain walls, including the heterophase walls that separate the near-interface polar phase from the remaining antiferroelectric matrix. Understanding these processes in better detail is required to extend the relatively well-established branch of ferroelectric thin film physics towards the less explored areas of large-mismatch perovskite heterostructures and of epitaxial antiferroelectrics.

This problem demands a structural characterization with *in situ* application of the electric field. To this end, a considerable experience has been accumulated with the bulk antiferroelectrics, predominantly PbZrO_3 modified by niobium, tin, and titanium (PNZST). In that system the switching field was considerably reduced (from hundreds to a few tens of kV/cm), enabling one to switch the ceramics before their dielectric breakdown occurred. The most direct experience seems to be that of Liu *et al.* [24], who captured the motion of heterophase domain walls that separate antiferroelectric and ferroelectric phases during switching. Slightly less direct, but still highly instructive examples are those of *in situ* electron [25,26], x-ray [27], and neutron [28] studies of PNZST ceramics and a rare diffraction study of a pure PbZrO_3 single crystal under an electric field by Shuvaeva *et al.* [29]. Also, single crystals of PbZrO_3 doped by titanium were recently studied by Vakhrušev *et al.* [30] under the influence of small (compared to the normal switching field) field, which nevertheless influenced the transitions due to high temperatures. The above works suggested a direct transition from the incommensurate AFE to the rhombohedral ferroelectric phase in PNSZT and PZT, while for pure PbZrO_3 one expects a sequence consisting of two orthorhombic (one of which was solved by Shuvaeva *et al.* [29]) and two rhombohedral field-induced phases [31]. Apparently, such *in situ* studies have not yet been applied to antiferroelectric thin films, although the switching in ferroelectric films has been studied using time-resolved synchrotron experiments [32,33].

Concerning the theories related to antiferroelectric switching, a consensual understanding has not yet been obtained. Recently, Lisenkov *et al.* [34] studied bulk PbZrO_3 using a combination of density functional theory (DFT) calculations of zero-K total energy and METROPOLIS Monte Carlo simulations. The authors reported field-induced transitions into ferroelectric phases with polarization roughly along those high-symmetry directions, along which the field was applied. This was different from what the experiments of Fesenko *et al.* [31] and Shuvaeva *et al.* [29] suggested. For each of the directions in molecular-dynamics study, there was a single transition without intermediate phases [34]. This mimics the earlier results of Fthenakis and Ponomareva [35], who studied specifically the (001)-oriented PbZrO_3 thin films by molecular dynamics and found a tetragonal field-induced phase. Notably, that molecular-dynamics work did not show any particular smearing of the P - E curves at relatively low field frequencies, at which the experimentalists saw the smearing [17–19]. So, the pioneering *ab initio* works on antiferroelectric switching do not yet match some essential aspects of the experiments, such as the specific symmetry of field-induced phases in crystals and smearing of antiferroelectric loops in films. As to the very stability of different structures in antiferroelectrics at zero K, there is also a set of standing points of order, such as the recent discoveries of alternative ground states of PbZrO_3 . In particular, Baker *et al.* [36] suggested an 80-atom $Pnam$ -symmetry alternative ground state, while Aramberri *et al.* [37] further suggested a ferroelectric alternative ground state with “down-up-up” ordering of lead-ion shifts. Those structures showed zero-K local energy minima slightly below that of the standard $Pbam$ -symmetry antiferroelectric phase. But there can be also other local minima that are slightly above it, indicating the competing metastable structures, such as the ones resembling incommensurate phases [38,39]. It seems that in DFT analysis of PbZrO_3 one may find numerous different competing local energy minima, and it is presently unclear whether the lowest of those does indeed point to the real ground state [36,37]. In films, only the minima related to $Pbam$ and $R3c$ structures were considered in detail [23,40]. Interestingly, those two studies pointed to different mechanisms of ferroelectric phase stabilization. Reyes-Lillo and Rabe [23] considered the effects of epitaxial strain, while Mani *et al.* [40] pointed to the effect related to purely local (related to individual ionic shifts) interactions disturbed at the interface between the film and vacuum.

This work characterizes (001)-oriented PbZrO_3 films, which are similar to those where smeared P - E loops have been observed [17–19], by single-crystal x-ray diffraction with *in situ* application of electric field. Due to the specifics of the method, the field values are precritical, that is, smaller than those needed to induce the transition to the ferroelectric phase. Nevertheless, distinct structural changes are evident, wherein the superstructural reflections with pseudocubic coordinates $\frac{1}{8}(1, 0, 1)$ and $\frac{3}{8}(1, 0, 1)$ appear and increase gradually with the field, while the original antiferroelectric reflections $\frac{1}{4}(1, 0, 1)$ decrease in intensity. By modeling of structure factors, we determine that the newly forming structure corresponds to an unusual lead-ion displacement pattern, which can be encoded as $\uparrow\uparrow\uparrow\uparrow\downarrow\uparrow\uparrow\downarrow$ (original antiferroelectric pattern [41] is $\downarrow\downarrow\uparrow\uparrow$ in this notation). This structure

is remarkably commensurate (as opposed to more common incommensurate phases [25,42–45]) and contains an uncommonly short-period main motif, manifested in lone “down” displacements surrounded by longer blocks of “up” displacements. This structure is polar and ferrielectric-like (hereafter the suffix “-like” is omitted for brevity, despite noting that the polarization is not spontaneous) in the sense of having incomplete compensation of oppositely directed dipoles. This makes its field-induced formation likely responsible for the unusually large effective dielectric constant deduced from P - E loops between more sharp switching events to the ferroelectric phase. Explaining the reason for this phase is a nontrivial task, at least the homogeneous strain, which we considered similarly to the authors or Refs. [23,46,47], does not seem responsible for it. Apparently, this is because the real polydomain and heterophase (antiferroelectric and ferrielectric phases coexist) configuration sets out a problem of a different kind, which is more related to the considerations of multiphase states in perovskites mediated by mechanical and electrical effects [48,49], as well as to the considerations of purely local interactions at the PbZrO_3 -vacuum interface [40]. A plausible explanation for the appearance of exactly the observed ferrielectric phase instead of the multitude of structural alternatives is obtained by accounting for the energy of the heterophase domain walls.

The results have a connection to prospective applications of antiferroelectric films by identifying an effect behind the P - E loops smearing. Also they are important for developing the physics of antiferroelectrics, in general, by revealing a seemingly unlikely structure suitable for a demanding benchmark of theoretical models. The work hints at the way towards creating and manipulating complex small-scale dipolar patterns that can be prospectively used in memories or other dense electronics.

II. METHODS

The experimental method is a single-crystal x-ray diffraction with *in situ* application of constant (not stroboscopic [32,33]) electric field. The details for that, as well as for sample synthesis and *ab initio* calculations are provided below, while the method of structure solution and semi-empirical energy analysis are provided in Secs. III and IV, respectively.

A. Thin film synthesis and basic characterization

We used (001)-oriented $\text{PbZrO}_3/\text{SrRuO}_3/\text{SrTiO}_3$ epitaxial heterostructures grown by pulsed-laser deposition at the University of California, Berkeley, as in earlier publications [50,51]. The SrRuO_3 was grown at a heater temperature of 680°C in a dynamic oxygen pressure of 100 mTorr and with a laser fluence and repetition rate of 1.0 J/cm^2 and 5 Hz, respectively. For the PbZrO_3 films, growth was completed at a heater temperature of 630°C in a dynamic oxygen pressure of 80 mTorr and with a laser fluence and repetition rate of 1.8 J/cm^2 and 5 Hz, respectively. The thickness of the PbZrO_3 and SrRuO_3 layers were 50 nm and 20 nm, respectively. The sputtering of the film has been done continuously (as

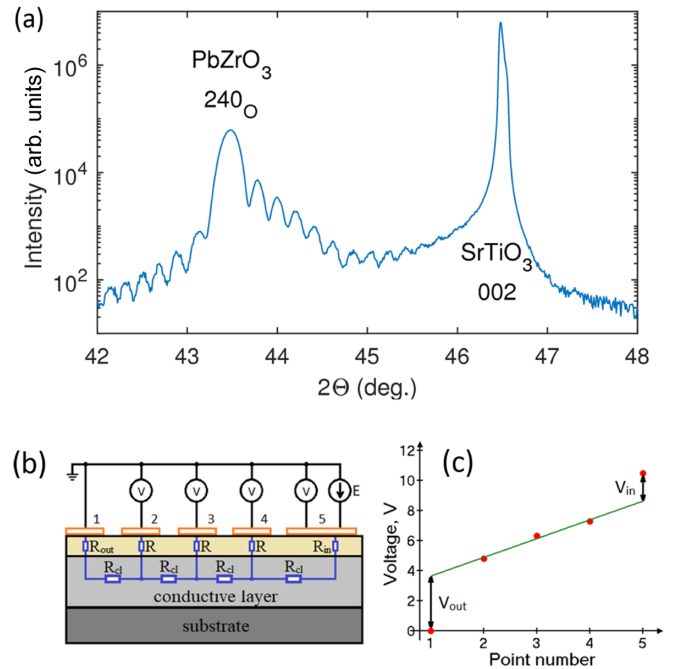


FIG. 1. Basic sample x-ray characterization and a scheme of *in situ* electric field application. (a) Standard θ - 2θ scan shows an asymmetry in the shoulders of the 240_O film reflection, well-defined Laue oscillations related the PbZrO_3 film, no well-defined oscillations from the SrRuO_3 layer. (b) Scheme of applying the field to the film. The electrodes 1 and 5 are the ground and active (diffraction) electrodes, respectively. Electrodes 2 to 4 serve for probing the potential in the conducting SrRuO_3 layer to determine the actual voltage drop under the active electrode. (c) Readings of the voltmeters and the linear extrapolation of the potential at electrodes 2 to 4 to the points 1 to 5, which allows determining the actual voltage drop under the active electrode.

contrasted to using cyclical breaks for intermediate surface recovery in a recent study of similar heterostructures on DyScO_3 substrate [19] by some of us).

The symmetric θ - 2θ x-ray diffraction scan [Fig. 1(a)], obtained with the Panalytical X’Pert 3 MRD system (UC Berkeley), shows the following points. First, there are well-defined Laue oscillations related to the PbZrO_3 layer, which indicate a good thickness homogeneity. More quantitatively, by correlating the sharpness of those oscillations with the reference calculations of Boule *et al.* [52], one obtains an estimate for the thickness fluctuations magnitude that does not exceed about 1 nm. Second, no specific oscillations related to the SrRuO_3 layer are seen. Tentatively, this is related to the rather strong imperfection of the $\text{PbZrO}_3/\text{SrRuO}_3$ interface. Third, the intensity shoulders on the left-hand and on the right-hand sides of the film’s reflection are asymmetric. From modeling of this asymmetry using the methodology of Ref. [52] in our previous work [51], it has been identified that this asymmetry corresponds to the near-interface out-of-plane compressive strain, which decays from few percents in magnitude at the interface to much less than a percent at the depth of 10 nm. The second and the third observations above are different from those in Ref. [19], which stems, tentatively, from the different substrates and deposition modes.

B. Application of field

To apply the external field, we used the conducting SrRuO₃ layer for the bottom electrode and sputtered 80 nm Au/4 nm Cr top electrodes. Diffraction experiments required relatively large electrodes, about 0.5 by 0.5 mm, which is much larger than the electrodes normally utilized for the electrical characterization of such thin films, which are typically tens of microns in size. The total resistivity of the devices is rather small, hundreds of Ohms, while the specific resistivity, about 2 Ohm/cm², is compatible with typical values for PZT films [53]. The relatively small resistivity requires a specific procedure for estimating the actual electric field under the illuminated electrode, which is done using a series of electrodes deposited along the line between the ground and illuminated electrodes, each of which has been measuring the potential of the SrRuO₃ layer at the respective points [Figs. 1(b) and 1(c)]. The potential below the illuminated electrode was estimated by a linear extrapolation through the readings of voltmeters connected to the intermediate electrodes.

This experimental approach has a limited accuracy of field determination, primarily due to the small ratio between the voltage drop under the diffraction electrode and total voltage drop between diffraction and ground electrodes, which is about 0.15 (the small error in the slope of the straight line in Fig. 1 leads to large error in V_{in}). The same amount of ferroelectric phase was observed in different 50-nm-thick samples at fields differing up to about two times.

The resistivity of the device was found to be constant as a function of voltage and time for fields up to about 200–300 kV/cm. At higher fields the samples degraded with time: about 10 percent resistivity loss in 30 minutes at E about 600–800 kV/cm. The measurements were carried in the DC regime, within the field range free from resistivity degradation. For this field range, the sample returns nearly to its initial condition upon switching off the field.

C. Diffraction measurements

The diffraction measurements were carried out using a SuperNova (Rigaku Oxford Diffraction) single-crystal diffractometer equipped with an ATLAS PSD detector. The film's normal was oriented along the rotation axis, the surface was oriented 15° with respect to the incoming beam (Cu K α , $\lambda = 1.5$ Å), the direction towards the detector was inclined by 60° with respect to the incoming beam. At each field value, the data were collected by rotating the film along the normal with exposure of 6 seconds per 1°.

D. *Ab initio* calculations

DFT calculations were performed using the Vienna *ab initio* simulation package (VASP) [54]. The projector augmented wave (PAW) potentials were used, with the generalized gradient approximation (GGA) and the Perdew-Burke-Ernzerhof (PBE) exchange-correlation functional for solid (PBEsol) [55]. The plane-wave cutoff energy was 500 eV. Lead 6s6p, zirconium 4s4p4d5s, and oxygen 2s2p states were treated as valence electrons. $6 \times 1 \times 4$ Monkhorst-Pack k -mesh was used, and the structures were fully optimized until all ionic forces in the system were within 0.001 eV/Å. The structures

and their respective energies that are shown in the text were obtained within a cell of the size $\sqrt{2} \times 12\sqrt{2} \times 2$, which is compatible with all the relevant modulation periods. Additionally, these calculations were verified by optimizing the same structures in smaller cells than the individual structures allow. The smaller-cell calculations provided visually the same results in the sense of atomic positions and the same energies within about 0.3 meV per formula unit.

III. RESULTS

Summarily, electric field creates additional superstructural reflections whose intensities are used to solve the structure and then to estimate the volume fractions of the newly created phase as a function of field. The commensurate modulated structure with regular lone “down” displacements forms in remarkably large amounts at precritical fields.

A. Superstructural reflections

When no field is applied, the film is populated with antiferroelectric domains with c -axes parallel to the film, while there are also diffraction signatures tentatively related to the near-interface layer of different structure. The related reciprocal space map is plotted in Fig. 2(a) (we plotted the pattern $E \approx 75$ kV/cm instead of basically identical zero-field map because of its better quality).

The diffraction pattern consists of the following.

- (i) Superstructural reflections with reduced wave vectors $\vec{q} = \frac{1}{4}(1, 0, 1)$ in pseudocubic coordinates where [001] points along the normal (Σ points);
- (ii) Reflections at $\frac{1}{2}(1, 1, 1)$ (R points); and
- (iii) At $\frac{1}{2}(1, 0, 1)$ (out-of-plane M points) and $\frac{1}{2}(1, 1, 0)$ (in-plane M points).

The Σ -point reflections are due to lead-ion displacements organized in a transverse wave with pattern $\downarrow\uparrow\uparrow\uparrow$. The R -point reflections are expected to be due to antiphase octahedral tilts according to the bulk PbZrO₃ structure [41], although a part of the R -point intensity could be also due to the antiphase lead displacements, as considered by Ricote *et al.* [56] for PZT.

The M -point reflections are less well understood. In PZT they were considered by Ricote *et al.* [56] as being due to either in-phase octahedral tilts or due to antiphase lead-ion displacements, while stressing that they are not compatible with the average rhombohedral $R3c$ ferroelectric structure and should be related to structural inhomogeneities in rhombohedral PZT. Our previous temperature-dependent x-ray diffraction study of the present samples has shown that the in-plane and out-of-plane M -point reflections have different temperature dependencies [50]. The exact microscopic nature of those reflections is not clear, although they are likely related to the near-interface layer with different structure. The M -point reflections are much weaker than those at Σ points.

Larger fields result in the appearance of superstructure reflections at $\frac{1}{8}(1, 0, 1)$ and $\frac{3}{8}(1, 0, 1)$ [Figs. 2(b), 2(e) and 2(f)]. These types of reflections in PbZrO₃ have not been previously observed and their origin is to be determined in this work. The intensity of these reflections increases gradually

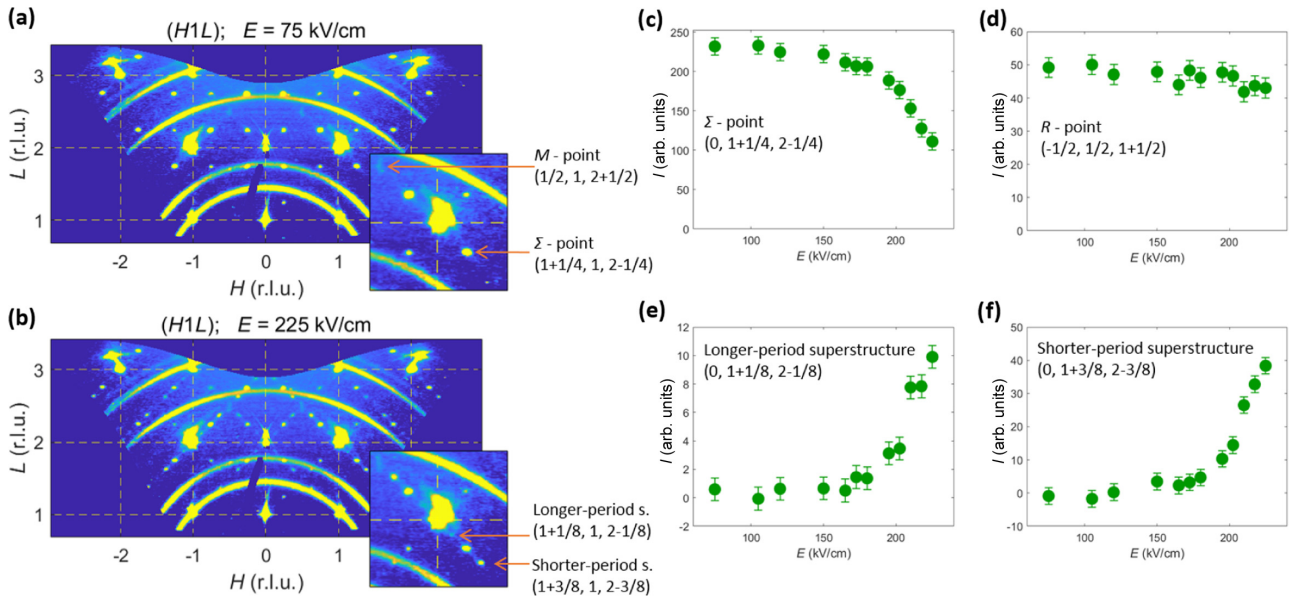


FIG. 2. Diffraction evidence for the gradual formation of long-period structure upon field increase in $\text{PbZrO}_3/\text{SrRuO}_3/\text{SrTiO}_3$ heterostructure. Panels (a,b) show reciprocal space maps at $E \approx 75$ kV/cm and $E \approx 225$ kV/cm, respectively. The second is still below the critical field for AFE-FE transition. Panels (c,d) show field dependence of intensity at Σ - and R -points, respectively. Panels (e,f) show field dependencies for reflections emerging on field increase. Powder rings correspond to the scattering by gold electrodes. Note that the field scale may differ considerably from device to device (see Sec. II).

with the field, while the intensity of reflections at $\frac{1}{4}(1, 0, 1)$ decreases [Fig. 2(c)]. The reflections at $\frac{3}{8}(1, 0, 1)$ are about six to seven times stronger than those at $\frac{1}{8}(1, 0, 1)$. The R -point peak is nearly field-independent [Fig. 2(d)], which should be interpreted as the oxygen octahedral tilt subsystem being largely unaffected in this field range. The M -point reflections also remain intact. Upon field removal, the diffraction pattern comes to nearly the initial state, although some reminiscent intensity remains detectable at $\frac{3}{8}(1, 0, 1)$. A mild hysteretic difference between the field dependencies on going forward and back is observed (this was measured in another device than in Fig. 2, with weaker statistics, and is not shown for brevity).

B. Solving the structure

The structure responsible for field-induced reflections is similar to the antiferroelectric structure, but with the lead-ion shift pattern being $\uparrow\uparrow\uparrow\uparrow\downarrow\uparrow\uparrow\downarrow$ instead of $\downarrow\downarrow\uparrow\uparrow$.

Identification of the actual structure that is responsible for the diffraction pattern is not straightforward because no well-established crystallographic workflows are available for thin films. We used the following approach, which is based on the brute-force enumeration of qualitatively different possible displacement patterns and evaluating their potential suitability for reproducing the observed intensities.

First, the unit cell was identified on the basis of the observed superstructural reflections. It has dimensions $\sqrt{2}a_{\text{pc}} \times 4\sqrt{2}a_{\text{pc}} \times 2a_{\text{pc}}$, which corresponds to the size of the antiferroelectric $Pbam$ unit cell that is twice enlarged along the b axis. Then the intensities of the superstructure spots were used to identify the ionic displacements. Since the R -point reflections do not react considerably to the field, the tilt pattern should

remain qualitatively intact, namely $a^-a^-c^0$ [57], where tilts occur around the a axis. As long as zirconium ions are not expected to shift considerably, it remains to identify the lead-ion displacements. These displacements are nearly parallel to the a axis, as the observability conditions for the superstructure reflections indicate (no visible reflections where the reduced and the total wave vector transfers are nearly parallel). Therefore, the lead-ion shift's pattern can be parametrized by eight real numbers, u_i (the number of lead-ion positions along the b axis). While the accurate refinement of all these numbers on the basis of recorded intensities seems unfeasible, it appears straightforward to extract the qualitative picture. For that, one invokes an assumption that all u_i are equal in magnitude, but can be different in their signs. Effectively, this reduces the refinement problem to finding those spin-like values $s_i = u_i/|u_i|$ that allow reproducing the diffraction pattern qualitatively. This task turns out to be well conditioned because the simulated diffraction pattern is very sensitive to s_i , while the experimental diffraction pattern is quite specific and an unusual one. There are only a few combinations that can produce the reflection at $\frac{3}{8}(1, 0, 1)$ larger than that at $\frac{1}{8}(1, 0, 1)$. Table I summarizes the structure determination procedure. In the end, the only potentially suitable structures are $\uparrow\uparrow\uparrow\uparrow\downarrow\uparrow\uparrow\downarrow$ and $\uparrow\downarrow\downarrow\uparrow\downarrow\uparrow\uparrow\downarrow$. From those two, one has to select the first because it has an uncompensated dipole moment, which makes it field sensitive.

Upon checking by DFT, we found a local energy minimum corresponding to this structure, which looks as depicted in Fig. 3(a). It has slightly (by a factor of about 0.7) smaller displacements of type “down” than those of type “up.” The “up” displacements are similar in magnitude to those in the standard PbZrO_3 antiferroelectric structure.

TABLE I. The 14 non-equivalent configurations of lead ion displacements with a period of eight and the superstructure reflection intensities they produce. By non-equivalent configurations we mean those that cannot be obtained from each other by cyclic shifts, flips and inversions. Also, this list does not include the configurations, which are effectively of smaller period (four or two or one). The structure factor has been calculated as $F = \sum_{j=1}^8 f(Q)\exp(i\vec{Q}\vec{r}_j)$, where j enumerates lead ions in the cell, $f(Q)$ is the atomic factor for lead. Lead ion positions were assumed as if all the displacements were by 0.28 \AA in magnitude (as in pure PbZrO_3), while the signs were determined by the displacement pattern. To be potentially consistent with the experiment, the structure has to result in zero intensity for $\xi = 1/2$ and provide the intensity for $\xi = 3/8$ larger than for $\xi = 1/8$. This is true only for configurations numbered 1 and 2. Among those, only the structure number 2 has non-zero net polarization, which makes it the likely structure that is experimentally observed.

Configuration number	Pb displacements configuration	$ F_{(-1+\xi, 0, 2+\xi)} ^2/10^4$, (number of electrons) ²			
		$\xi = \frac{1}{8}$	$\xi = \frac{1}{4}$	$\xi = \frac{3}{8}$	$\xi = \frac{1}{2}$
1	$\uparrow\downarrow\downarrow\downarrow\uparrow\uparrow\downarrow$	1.23	0	6.97	0
2	$\uparrow\uparrow\uparrow\uparrow\downarrow\uparrow\uparrow\downarrow$	0.61	2.07	3.48	0
3	$\uparrow\uparrow\downarrow\downarrow\uparrow\downarrow\downarrow\downarrow$	2.10	4.14	2.04	0
4	$\uparrow\uparrow\downarrow\downarrow\downarrow\uparrow\downarrow\downarrow$	0.61	2.07	3.48	4.01
5	$\uparrow\uparrow\uparrow\uparrow\downarrow\downarrow\downarrow\downarrow$	7.16	0	1.20	0
6	$\uparrow\uparrow\uparrow\uparrow\uparrow\downarrow\downarrow\downarrow$	6.11	1.04	0.18	1.00
7	$\uparrow\uparrow\uparrow\uparrow\downarrow\uparrow\downarrow\downarrow$	3.14	1.04	3.06	1.00
8	$\uparrow\uparrow\uparrow\downarrow\uparrow\uparrow\downarrow\downarrow$	1.05	5.17	1.02	1.00
9	$\uparrow\uparrow\uparrow\downarrow\uparrow\downarrow\uparrow\downarrow$	1.05	1.04	1.02	9.03
10	$\uparrow\uparrow\downarrow\uparrow\uparrow\downarrow\uparrow\downarrow$	0.18	1.04	5.95	1.00
11	$\uparrow\uparrow\uparrow\uparrow\uparrow\uparrow\downarrow\downarrow$	3.58	2.07	0.60	0
12	$\uparrow\uparrow\uparrow\uparrow\uparrow\downarrow\uparrow\downarrow$	2.10	0	2.04	4.01
13	$\uparrow\uparrow\uparrow\uparrow\downarrow\downarrow\downarrow\downarrow$	3.58	2.07	0.60	4.01
14	$\uparrow\uparrow\uparrow\uparrow\uparrow\uparrow\uparrow\downarrow$	1.05	1.04	1.02	1.00

C. Volume share as a function of field

Intensities of superstructure reflections allow one to compute the volume share of the ferrielectric phase at different field values. To do so, one needs to work with three reflections: at $\frac{3}{8}(1, 0, 1)$ and $\frac{1}{8}(1, 0, 1)$, to which only the ferrielectric phase contributes, and at $\frac{1}{4}(1, 0, 1)$, to which both the antiferroelectric and the ferrielectric phases contribute. By knowing the theoretically computed ratios of structure factors related to these contributions (see Table I), it is straightforward to compute the field dependence of the ferrielectric phase volume share, as the inset in Fig. 3(b) shows. The formulas used for the computation are listed in the Appendix.

The volume share of ferrielectric domains $n(E)$ is rather large, about a half of the film's volume, at the largest field applied (about 220 kV/cm). This field is still below the critical field of antiferroelectric-to-ferroelectric switching. The latter is estimated as about 250 kV/cm [18]. If one assumes that the antiferroelectric phase occupies the volume share $[1 - n(E)]$, the modeled superstructure reflection intensities agree well with the experiment [see Fig. 3(b)]. This suggests that the field-induced changes are related mainly to the redistribution

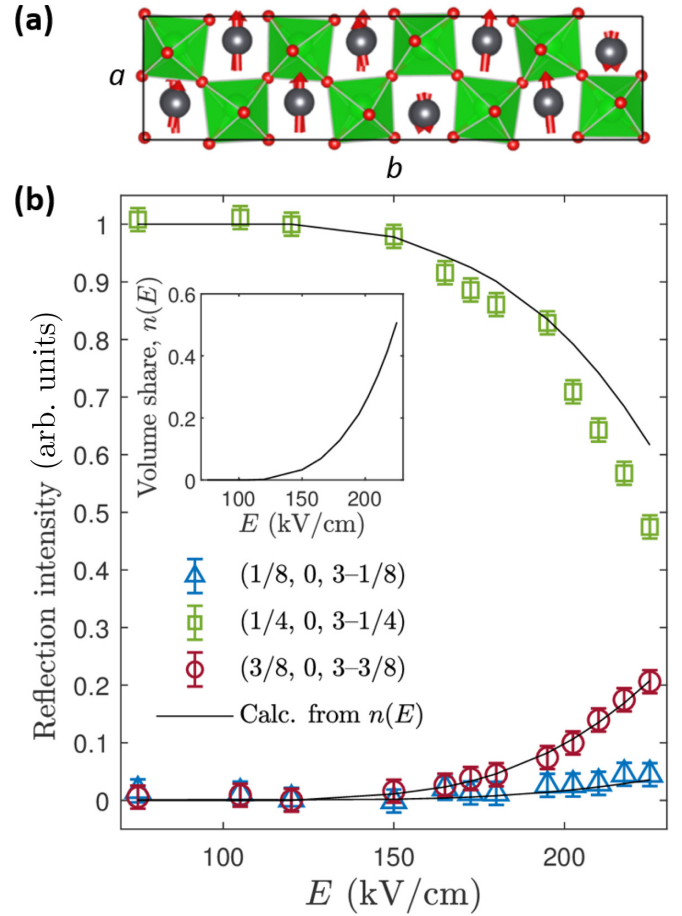


FIG. 3. (a) Unit cell of the ferrielectric structure, as determined by DFT simulation. Arrows show the direction and relative magnitude of lead-ion displacements. (b) Volume share of the ferrielectric phase as a function of the field (inset), as calculated from the intensities of reflections that are specific to the ferrielectric phase (circles and triangles). Squares stand for the intensity of reflection at $\vec{q} = (1/4, 1/4, 0)$, to which both the ferrielectric and the antiferroelectric structures contribute.

of the volume between the antiferroelectric and the newly formed phases, while the volume of the ferroelectric phase (which is believed to be near the interface) changes only a little.

IV. INTERPRETATION

The field-induced structure with displacement pattern $\uparrow\uparrow\uparrow\downarrow\uparrow\uparrow\downarrow$ is similar to the alternative ground state of Aramberri *et al.* [37] with displacement pattern $\downarrow\uparrow\uparrow$ in the sense of having lone “down” displacements surrounded by larger blocks of “up” displacements. The difference is that the field-induced structure has four- and two-cell-long “up” blocks, which are regularly interchanged, while it is all the time two unit cells for the $\downarrow\uparrow\uparrow$ structure. The reason for this difference is likely the energy of the heterophase domain walls, which makes the $\downarrow\uparrow\uparrow$ structure unfavorable, but allows its main lone-“down” displacement motif to be incorporated into the observed eight-unit-cell period with small energy penalty.

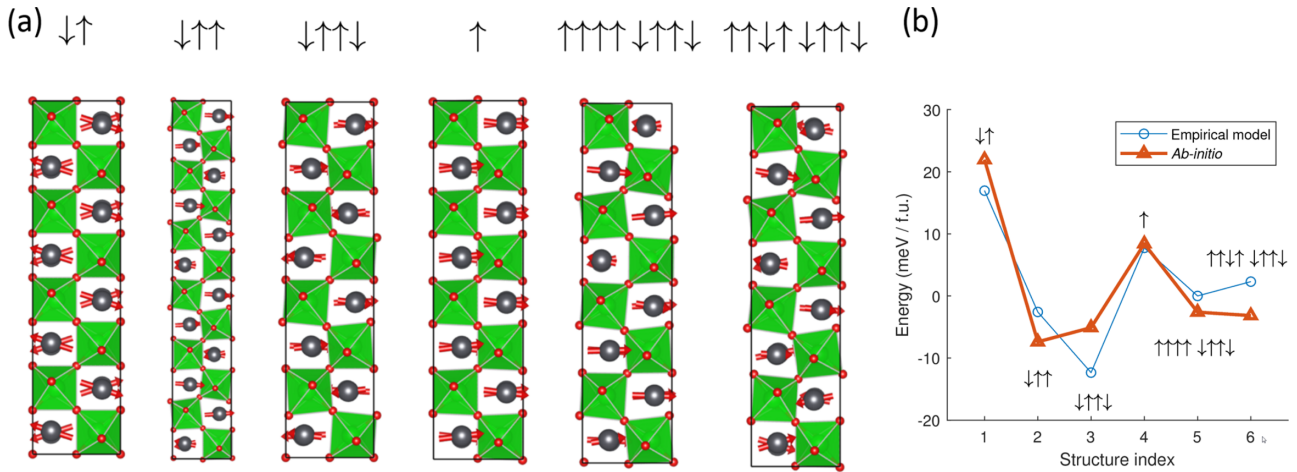


FIG. 4. Structures with different lead-ion displacement patterns, as obtained by DFT (a), and their respective energies (b). Only those structures are listed that enter the phase diagram in Fig. 6. The energy in the plot is per formula unit. Cubic structure (not shown) has energy of 319 meV/f.u. on this scale.

A. *Ab initio* energies

We examined a few related structures using *ab initio* calculations by setting manually their desired displacement patterns and then letting the structure optimize towards the respective local energy minimum. The structures and respective energies are shown in Fig. 4. These results confirm the lowest energy of the $\downarrow\uparrow\uparrow$ pattern (it is not yet fully clear why it is so [37]), which is tightly followed by the antiferroelectric pattern $\downarrow\downarrow\uparrow\uparrow$, while showing large energies for ultra-short- and ultra-long-period patterns $\downarrow\uparrow$ and \uparrow . The ultra-long-period corresponds to the orthorhombic ferroelectric phase, which is different from the one solved by Shuvaeva *et al.* [29]. The experimentally observed field-induced structure (index 5) has an intermediate energy. Applying different homogeneous strains to these unit cells (not shown [58]) does not reveal a preference to the desired structure over the others, which suggests that strain is not its direct driving factor. This can be logical because the actual picture of epitaxial strain in this type of heterostructures is more complex than just a homogeneous strain. Such films are strongly relaxed [18,19], which leaves only a small portion of the remnant strain sufficiently away from the interface [4,59], while the near-interface layer can be subject to inhomogeneous elasto-electric effects related to dislocations [60,61]. Furthermore, the away-from-the-interface part of the film is in the polydomain state and individual domains should experience custom strains due to their mutual elastic interaction via the substrate [62,63]; these strains are expected to be different from the average remnant strain. Why the observed structure appears in films, while not appearing in the bulk PbZrO_3 , does not become clear upon basic bulk-like *ab initio* modeling. A more specialized consideration seems necessary, as follows.

B. Energy of heterophase boundary

The period of eight cells seems unnatural for the observed structure because the main structural motif (lone “down” and few “up” displacements) is much shorter. This suggests an external factor being, in effect, to pack that motif into a longer period. The most natural factor of this sort

are heterophase boundaries between field-induced and antiferroelectric phases. Their energies can be important in nanodomain structures and, as we see below, such boundaries can commensurate the period of the field-induced phase (eight) with that of the antiferroelectric phase (four).

A hint comes from the simplified two-dimensional consideration of a horizontal heterophase boundary in Fig. 5. It shows layers of lead-ion displacements that propagate from one phase to the other. When they propagate intactly (the

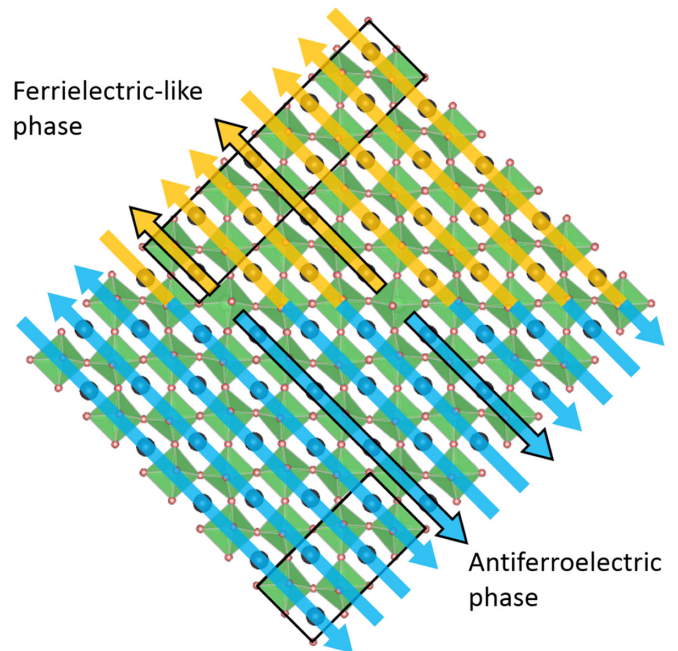


FIG. 5. Contact between the field-induced phase and the antiferroelectric phase. The respective unit cells are contoured out. Arrows show the directions of lead ion displacements in the layers. Highlighted arrows correspond to the layers, where the displacement direction is reversed at the interphase boundary. Mathematically, such a picture can be interpreted as antiferroelectric phase exerting antiferroelectric field onto the field-induced phase.

direction of displacement is not changed between phases), this costs no energy, while when they break, one expects it to have a cost. Let this cost to be B for each broken layer, the wall energy will be B times the number of broken layers. When $s_i = \pm 1$ stand for displacement directions in the field-induced phase and v_i are in the antiferroelectric phase, the boundary energy will be

$$W_B = B/2 \sum_{i=1}^N (1 - v_i s_i) = NB/2 - \sum_i [(B/2)v_i] s_i. \quad (1)$$

The term $NB/2$ stands for the energy of a wall between structures with mutually random displacements, while the term next to it stands for covariance between displacement patterns. Covariance, and hence an energy gain or loss with respect to the random-pattern case, can be nonzero if the structures are commensurate with each other, while in the incommensurate case this term cancels. This explains why the field-induced phase can become commensurate with the antiferroelectric phase instead of being incommensurate with a similar period, such as the ones observed in related materials [25,42–45].

C. Modeling insights

Understanding the commensuration effect of the heterophase boundary, as discussed above, is helpful, but leaves yet unclear why a particular commensurate pattern $\uparrow\uparrow\uparrow\downarrow$ is observed instead of other alternative commensurate-with-AFE patterns with uncompensated polarization, such as $\uparrow\uparrow\uparrow\uparrow\downarrow\downarrow$, which is more similar to common long-period structures in related materials [25]. A simple energy model that accounts for electric field, heterophase boundaries, and empirically parametrized displacement-displacement energy helps reduce this ambiguity. It suggests that among the commensurate-with-AFE displacement patterns, PbZrO_3 should likely go to either homogeneous polarization or to the observed field-induced structure upon field increase, depending on the particularities of the effective Hamiltonian.

In modeling, we take the perspective of the regions where the field-induced phase develops [where displacement directions denoted as s_i in Eq. (1)], while the other regions are assumed to be in the antiferroelectric phase, as the experiment suggests. The energy of heterophase boundaries can be modeled using an artificially introduced *antiferroelectric field* which acts externally on s_i . This field can be identified in the covariance term of Eq. (1) as $a_i = (B/2)v_i$ because it enters the energy function bilinearly with the displacements as $a_i s_i$, as the field should, and its i -dependence is the same as for antiferroelectric displacements, v_i .

We consider only that electric-field component which is parallel to the displacement direction (a axis of the cell, $[10\bar{1}]$ pseudocubic direction) and label it h . The other component of the field along the b axis ($[101]$) is neglected. The empirical formula for displacement-displacement energy is

$$W = \sum_i s_i \cdot (J_1 s_{i+1} + J_2 s_{i+2} + h + a_i). \quad (2)$$

Constants J_1 and J_2 describe the nearest-neighbor and next-nearest-neighbor interactions, respectively, as in the paper of

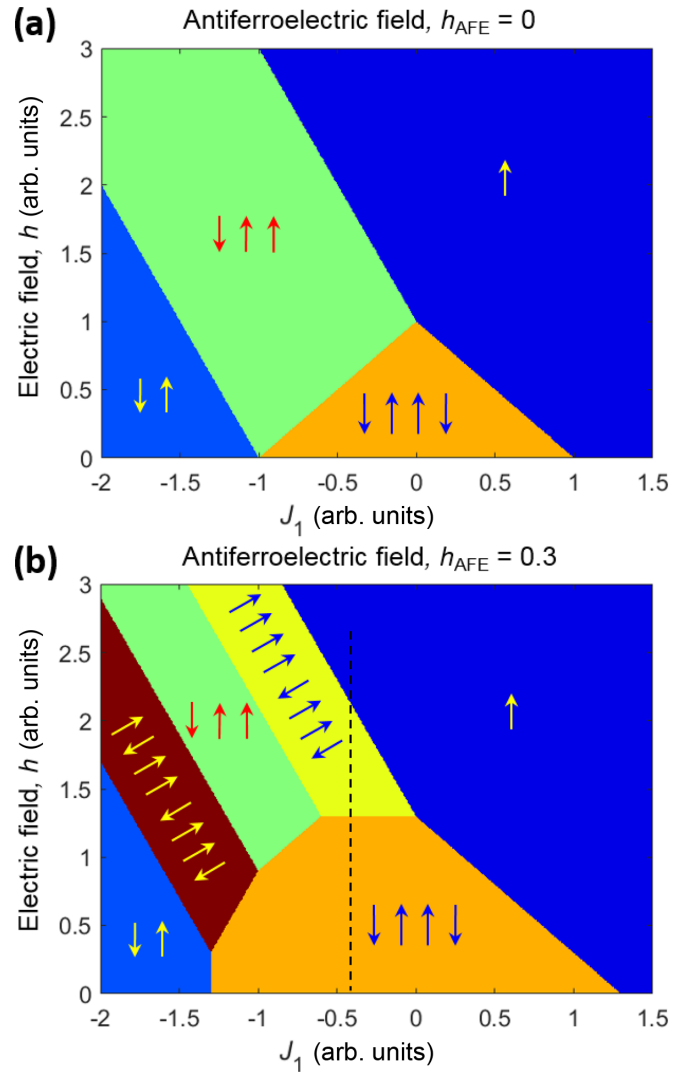


FIG. 6. Model phase diagram of an antiferroelectric in coordinates of electric field, antiferroelectric field, and tendency towards shorter or longer period modulations. Positive J_1 corresponds to the longer period modulations, while negative J_1 corresponds to the shorter period modulations. Another parameter of the model J_2 is taken as -0.5 . Dashed line shows a tentative path traversed by the system on changing the electric field (the change of interphase boundary position with field is neglected in plotting this trajectory).

Bak and Boehm [64]. This formula is used to check the energy of arbitrary $\{s_i\}$ configurations, which are not necessarily commensurate with a_i , so no cyclic boundary condition is possible, in general, and the summation is made over a wide i range to make the truncation-dependent contributions at the range ends negligible.

The formula agrees reasonably well with *ab initio* energies [see Fig. 4(b)], at least for the qualitative assessment that is being pursued. The estimates for J_1 and J_2 from the fit with both fields zero are 5 and -12 meV, respectively. Only their ratio is important for the analysis below, so we model the energies with J_2 fixed at -0.5 (for convenient comparison with Ref. [64]), while allowing J_1 to vary around its rescaled starting value of $(-0.5)5/(-12) \approx 0.2$.

The phase diagram in Fig. 6 tells how the minimal-energy displacement pattern depends on electric (h), and antiferroelectric ($h_{\text{AFE}} = |a_i|$) fields, and on the phenomenological constant J_1 . This constant, as can be seen, controls how much the system likes homogeneous polarization. For accepting lone “down” displacements, J_1 needs to be negative. The antiferroelectric phase is stable around zero J_1 and zero h , the orthorhombic ferroelectric phase is stable at high h , and the experimentally observed field-induced structure is stable between the antiferroelectric and ferroelectric phases (along the h axis) when the antiferroelectric field is nonzero. It is seen that when the antiferroelectric field is present, the system goes either directly to the ferroelectric phase, if J_1 is positive, or via the $\uparrow\uparrow\uparrow\uparrow\downarrow\uparrow\uparrow\downarrow$ pattern, when J_1 is only slightly negative. The *ab initio* estimation of $J_1 \approx 0.2$ is close to the boundary between these two scenarios.

It is not shown in the figure, but the structure $\uparrow\uparrow\uparrow\uparrow\downarrow\uparrow\uparrow\downarrow$ is energy-degenerate with the $\uparrow\uparrow\uparrow\downarrow$ structure, in which the lone “down” displacement is shifted. This is because the displacements in the model do not interact further than two neighbors away from each other. In reality this degeneracy is likely removed by more delicate effects.

V. DISCUSSION

The results have enabled us to identify the field-induced structure and suggest a role of heterophase contact in its stabilization. This stimulates a number of questions and perspectives, which we discuss below.

The symmetry of field-induced phases in PbZrO_3 are intriguing generally, in part, because of an incomplete agreement between experiments [31] and theory [34]. In films, quite probably [17], the switching takes place to the rhombohedral ferroelectric phase. Our study does not see the complete switching to the rhombohedral phase because it does not go that far in field, but sees the gradual formation of an orthorhombic phase, which is similar to the antiferroelectric one, but differs by the modulation period and pattern. Natural questions would be on why the rhombohedral phase, which already exists, as it is believed [18], in the near-interface layer, does not just expand its volume towards the rest of the film upon field increase, and why an orthorhombic ferroelectric phase expands instead.

The rhombohedral phase cannot expand outside the near-interface layer likely because that layer is a special place, modified substantially by dislocations and could be, in fact, polarized because of them through the flexoelectric effect [60]. Away from this strongly modified layer, the film should be more similar to the bulk, except for the dense domain configuration because, at least, of the elastic effects [62]. This part should naturally wait for a critical field before the rhombohedral phase might form. Normally, during this waiting, the system should react to field only by weak redistribution of ions and electrons within the same antiferroelectric phase, thus no more substantial changes should occur.

Experimentally, the structure changes in some regions, suggesting that these regions are different due to a sort of material inhomogeneity. Being different, these regions have the antiferroelectric structure less stable to the degree that in the absence of field they still retain it, but when the field

increases, they try finding alternative structures with uncompensated polarization, ending up in the observed ferroelectric pattern. The rhombohedral ferroelectric phase is, apparently, not among the primary candidates, possibly due to its worse mechanical compatibility with orthorhombic antiferroelectric surrounding.

The origin of inhomogeneity in $\text{PbZrO}_3/\text{SrRuO}_3/\text{SrTiO}_3$ heterostructures is yet unclear, although few tentative scenarios can be seen. First, structural heterogeneity can arise in films spontaneously due to elastic and possibly other effects, as emerges in phase-field modeling [65,66] and more classical considerations [49] of ferroelectric films. A similar scenario might be relevant also in antiferroelectric films, although the model should be more complex due to the numerous possible displacement patterns, as contrasted to only a few polarization directions in ferroelectrics. Alternatively, the structural heterogeneity might be imposed by the microstructure of the film. For example, the recent study of polycrystalline PbZrO_3 films by Lu *et al.* [67] suggested that physical grains might determine the domain sizes there. The present films are, in contrast, single-crystalline and do not have grains, so that particular scenario is not likely to be applicable. However, these films have a high density of dislocations (about each 7 nm, as dictated by lattice mismatch and as has been observed experimentally in similar samples [18]), so the corresponding inhomogeneous elastic fields from dislocation, as considered, for example, by Alpay *et al.* [61], may contribute to the structural heterogeneity. Another driver for the heterogeneity might be the inhomogeneous defect concentration or the interaction of film’s tilt subsystem with that of polydomain SrRuO_3 [68,69].

These possible specifics have not been considered explicitly in our analysis and modeling, as we assumed the inhomogeneity as granted by this or another way, simplifying further that heterophase domain walls are fixed. This simplification allowed us to identify the commensuralizing effect of heterophase boundaries and examine the potential field-induced structures in structure-changing regions. The modeling results suggest that structure-changing regions are modified in a way that lone “down” displacements (like in Aramberri *et al.*’s structure [37]) are slightly preferred over the standard “down-down-up-up” ordering and over large “up” and “down” blocks (as in the incommensurate phases [25]), and once it is so, the observed structure is surprisingly likely to appear instead of the other polar structures.

VI. CONCLUSION

Epitaxial films of PbZrO_3 on $\text{SrRuO}_3/\text{SrTiO}_3$ substrate react peculiarly to the relatively small constant electric fields. Instead of keeping the antiferroelectric phase until reaching the critical field for switching, a heterophase state forms and develops gradually with changing field. The forming structure is polar, which likely explains, at least in part, the unusually large effective dielectric constant in these films as extracted from P - E loops between antiferroelectric-ferroelectric switching events. The structure of the field-induced phase is unusual and stimulates interesting approaches for rationalizing it. To this end we suggested a key role of heterophase boundaries, which can commensuralize the

forming phase with the existing antiferroelectric phase. Further, we proposed a simple *ab-initio*-correlated empirical model showing that the orthorhombic ferroelectric and the observed ferrielectric phases are the two most likely options for a field-induced phase, provided that the cell is restricted to remain similar to the antiferroelectric phase, except for varying the modulation period and pattern. It seems required that the regions, where the ferrielectric phase develops, should have less stable antiferroelectric phase and a slightly larger tendency towards lone “down” displacements, as compared to the surrounding regions, which may be due to a rather large set of yet unexplored effects. The results allow understanding better the functional behavior of antiferroelectric heterostructures from a structural point of view and provide a step towards exploiting the related unusual effects in prospective applications, such as memory and energy storage.

ACKNOWLEDGMENTS

M. Alexe and A. K. Tagantsev are acknowledged for useful discussions. R.G.B., G.A.L., and A.E.G. acknowledge the support of the Russian Science Foundation (Grant No. 20-72-10126) for the experimental work (apart from thin film synthesis) and interpretation (apart from first-principles analysis). B.X. acknowledges financial support from National Natural Science Foundation of China under Grant No. 12074277 and Natural Science Foundation of Jiangsu Province (BK20201404) for performing first-principles analysis. Thin film samples were synthesized at UC Berkeley. R.G. acknowledges support from the National Science Foundation under Grant No. DMR-2102895. A.D. acknowledges support from the National Science Foundation under Grant No. DMR-1708615. L.W.M. acknowledges support from the Army Research Office under Grant No. W911NF-21-1-0118.

APPENDIX: DETERMINING THE VOLUME SHARE OF FERRIELECTRIC-LIKE STRUCTURE AS A FUNCTION OF FIELD

Experimentally, we observe a two-phase state in which the shares of antiferroelectric and ferrielectric phases change

with applied electric field. Here, we show how the volume shares of these phase are extracted from the diffraction picture.

Only the ferrielectric structure contributes to the reflections at $\frac{1}{8}(1, 0, 1)$ and $\frac{3}{8}(1, 0, 1)$, while both the ferrielectric structure and AFE structure contribute at $\frac{1}{4}(1, 0, 1)$. The contribution of each structure (ferrielectric and AFE) to the intensity at particular \vec{q} is proportional to the volume fraction of this structure and to the squared absolute value of the relevant structure factor $|F|^2$. The field dependence of the ferrielectric phase volume fraction, $\eta_X(E)$, can be calculated using the following formulas:

$$I_{1/8}(E) = \eta_X(E) |F_{1/8}^X|^2 k, \quad (\text{A1})$$

$$I_{3/8}(E) = \eta_X(E) |F_{3/8}^X|^2 k, \quad (\text{A2})$$

$$I_{1/4}(E) = ([1 - \eta_X(E)] |F_{1/4}^{\text{AFE}}|^2 + \eta_X(E) |F_{1/4}^X|^2) k, \quad (\text{A3})$$

where the k —a constant proportional to the beam intensity F_ξ^X —structure factor of the ferrielectric structure at the $\vec{q} = (\xi, \xi, 0)$ point of reciprocal space and $F_{1/4}^{\text{AFE}}$ —the structure factor of the AFE structure at the Σ point.

There is no ferrielectric structure at zero field. The entire volume is in the AFE phase [$\eta_X(E=0) = 0$]. Substituting this to Eq. (A3), one obtains the constant k as

$$k = \frac{I_{1/4}(0)}{|F_{1/4}^{\text{AFE}}|^2}. \quad (\text{A4})$$

The volume fraction of the ferrielectric phase $\eta_X(E)$ is derived from Eqns. (A2) and (A4) as

$$\eta_X(E) = \frac{I_{3/8}(E) |F_{1/4}^{\text{AFE}}|^2}{I_{1/4}(0) |F_{3/8}^X|^2}. \quad (\text{A5})$$

In the above formula, we used only $\frac{3}{8}(1, 0, 1)$ reflection since its larger intensity is better determined experimentally [the calculation agrees with the experiment also at $\frac{1}{8}(1, 0, 1)$, but this is much less informative due to low intensity].

-
- [1] M. Dawber, K. M. Rabe, and J. F. Scott, Physics of thin-film ferroelectric oxides, *Rev. Mod. Phys.* **77**, 1083 (2005).
- [2] N. Setter, D. Damjanovic, L. Eng, G. Fox, S. Gevorgian, S. Hong, A. Kingon, H. Kohlstedt, N. Park, G. Stephenson, I. Stolitchnov, A. K. Tagantsev, D. V. Taylor, T. Yamada, and S. Streiffer, Ferroelectric thin films: Review of materials, properties, and applications, *J. Appl. Phys.* **100**, 051606 (2006).
- [3] L. W. Martin and A. M. Rappe, Thin-film ferroelectric materials and their applications, *Nat. Rev. Mater.* **2**, 16087 (2017).
- [4] A. K. Tagantsev, L. E. Cross, and J. Fousek, *Domains in Ferroic Crystals and Thin Films* (Springer, New York, 2010).
- [5] M. Stengel and N. A. Spaldin, Origin of the dielectric dead layer in nanoscale capacitors, *Nature (London)* **443**, 679 (2006).
- [6] L.-W. Chang, M. Alexe, J. F. Scott, and J. M. Gregg, Settling the “dead layer” debate in nanoscale capacitors, *Adv. Mater.* **21**, 4911 (2009).
- [7] A. Yadav, C. Nelson, S. Hsu, Z. Hong, J. Clarkson, C. Schlepütz, A. Damodaran, P. Shafer, E. Arenholz, L. Dedon, D. Chen, A. Vishwanath, A. M. Minor, L. Q. Chen, J. F. Scott, L. W. Martin, and R. Ramesh, Observation of polar vortices in oxide superlattices, *Nature (London)* **530**, 198 (2016).
- [8] S. Das, Y. Tang, Z. Hong, M. Gonçalves, M. McCarter, C. Klewe, K. Nguyen, F. Gómez-Ortiz, P. Shafer, E. Arenholz, V. A. Stoica, S.-L. Hsu, B. Wang, C. Ophus, J. F. Liu, C. T. Nelson, S. Saremi, B. Prasad, A. B. Mei, D. G. Schlom, J. Íñiguez, P. García-Fernández, D. A. Muller, L. Q. Chen, J. Junquera, L. W. Martin, and R. Ramesh, Observation of room-temperature polar skyrmions, *Nature (London)* **568**, 368 (2019).
- [9] X. Wei, A. Tagantsev, A. Kvasov, K. Roleder, C. Jia, and N. Setter, Ferroelectric translational antiphase boundaries in non-polar materials, *Nat. Commun.* **5**, 3031 (2014).

- [10] M. Petic, S. Knebel, M. Hoffmann, C. Richter, T. Mikolajick, and U. Schroeder, How to make DRAM non-volatile? Antiferroelectrics: A new paradigm for universal memories, in *2016 IEEE International Electron Devices Meeting (IEDM)* (IEEE, New York, 2016), pp. 11.6.1–11.6.4.
- [11] Y. Zhang, X. Li, J. Song, S. Zhang, J. Wang, X. Dai, B. Liu, G. Dong, and L. Zhao, AgNbO_3 antiferroelectric film with high energy storage performance, *J. Materiomics* **7**, 1294 (2021).
- [12] M.-F. Tsai, Y.-Z. Zheng, S.-C. Lu, J.-D. Zheng, H. Pan, C.-G. Duan, P. Yu, R. Huang, and Y.-H. Chu, Antiferroelectric anisotropy of epitaxial PbHfO_3 films for flexible energy storage, *Adv. Funct. Mater.* **31**, 2105060 (2021).
- [13] X.-X. Huang, T.-F. Zhang, W. Wang, P.-Z. Ge, and X.-G. Tang, Tailoring energy-storage performance in antiferroelectric PbHfO_3 thin films, *Mater. Des.* **204**, 109666 (2021).
- [14] M. Guo, M. Wu, W. Gao, B. Sun, and X. Lou, Giant negative electrocaloric effect in antiferroelectric PbZrO_3 thin films in an ultra-low temperature range, *J. Mater. Chem. C* **7**, 617 (2019).
- [15] X.-X. Huang, T.-F. Zhang, R.-Z. Gao, H.-B. Huang, P.-Z. Ge, H. Tang, and X.-G. Tang, Large room temperature negative electrocaloric effect in novel antiferroelectric PbHfO_3 films, *ACS Appl. Mater. Interfaces* **13**, 21331 (2021).
- [16] K. Boldyreva, D. Bao, G. L. Rhun, L. Pintilie, M. Alexe, and D. Hesse, Microstructure and electrical properties of (120) O-oriented and of (001) O-oriented epitaxial antiferroelectric PbZrO_3 thin films on (100) SrTiO_3 substrates covered with different oxide bottom electrodes, *J. Appl. Phys.* **102**, 044111 (2007).
- [17] L. Pintilie, K. Boldyreva, M. Alexe, and D. Hesse, Coexistence of ferroelectricity and antiferroelectricity in epitaxial PbZrO_3 films with different orientations, *J. Appl. Phys.* **103**, 024101 (2008).
- [18] A. R. Chaudhuri, M. Arredondo, A. Hähnel, A. Morelli, M. Becker, M. Alexe, and I. Vrejoiu, Epitaxial strain stabilization of a ferroelectric phase in PbZrO_3 thin films, *Phys. Rev. B* **84**, 054112 (2011).
- [19] R. Gao, S. E. Reyes-Lillo, R. Xu, A. Dasgupta, Y. Dong, L. R. Dedon, J. Kim, S. Saremi, Z. Chen, C. R. Serrao, H. Zhou, J. B. Neaton, and L. W. Martin, Ferroelectricity in $\text{Pb}_{(1+\delta)}\text{ZrO}_3$ thin films, *Chem. Mater.* **29**, 6544 (2017).
- [20] X. Hao, J. Zhai, and X. Yao, Improved energy storage performance and fatigue endurance of Sr-doped PbZrO_3 antiferroelectric thin films, *J. Am. Ceram. Soc.* **92**, 1133 (2009).
- [21] M. D. Nguyen, T. T. Trinh, H. T. Dang, and H. N. Vu, Understanding the effects of electric-field-induced phase transition and polarization loop behavior on the energy storage performance of antiferroelectric PbZrO_3 thin films, *Thin Solid Films* **697**, 137794 (2020).
- [22] L. Jin, F. Li, and S. Zhang, Decoding the fingerprint of ferroelectric loops: Comprehension of the material properties and structures, *J. Am. Ceram. Soc.* **97**, 1 (2014).
- [23] S. E. Reyes-Lillo and K. M. Rabe, Antiferroelectricity and ferroelectricity in epitaxially strained PbZrO_3 from first principles, *Phys. Rev. B* **88**, 180102(R) (2013).
- [24] B. Liu, X. Tian, L. Zhou, and X. Tan, Motion of phase boundary during antiferroelectric–ferroelectric transition in a PbZrO_3 -based ceramic, *Phys. Rev. Materials* **4**, 104417 (2020).
- [25] H. He and X. Tan, Electric-field-induced transformation of incommensurate modulations in antiferroelectric $\text{Pb}_{0.99}\text{Nb}_{0.02}[(\text{Zr}_{1-x}\text{Sn}_x)_{1-y}\text{Ti}_y]_{0.98}\text{O}_3$, *Phys. Rev. B* **72**, 024102 (2005).
- [26] H. Guo and X. Tan, Direct observation of the recovery of an antiferroelectric phase during polarization reversal of an induced ferroelectric phase, *Phys. Rev. B* **91**, 144104 (2015).
- [27] H. Liu, L. Fan, S. Sun, K. Lin, Y. Ren, X. Tan, X. Xing, and J. Chen, Electric-field-induced structure and domain texture evolution in PbZrO_3 -based antiferroelectric by in-situ high-energy synchrotron x-ray diffraction, *Acta Mater.* **184**, 41 (2020).
- [28] T. Lu, A. J. Studer, D. Yu, R. L. Withers, Y. Feng, H. Chen, S. S. Islam, Z. Xu, and Y. Liu, Critical role of the coupling between the octahedral rotation and A-site ionic displacements in PbZrO_3 -based antiferroelectric materials investigated by in situ neutron diffraction, *Phys. Rev. B* **96**, 214108 (2017).
- [29] V. Shuvaeva, M. Y. Antipin, O. Fesenko, and Y. T. Struchkov, An x-ray diffraction and EXAFS study of the electric-field-induced PbZrO_3 ferroelectric phase, *J. Phys.: Condens. Matter* **8**, 1615 (1996).
- [30] S. B. Vakhruhev, D. Andronikova, I. Bronwald, E. Y. Koroleva, D. Chernyshov, A. V. Filimonov, S. A. Udovenko, A. I. Rudskoy, D. Ishikawa, A. Q. R. Baron, A. Bosak, I. N. Leontiev, and A. K. Tagantsev, Electric field control of antiferroelectric domain pattern, *Phys. Rev. B* **103**, 214108 (2021).
- [31] O. Fesenko, R. Kolesova, and Y. G. Sineyev, The structural phase transitions in lead zirconate in super-high electric fields, *Ferroelectrics* **20**, 177 (1978).
- [32] Y. Ehara, S. Yasui, T. Oikawa, T. Shiraishi, T. Shimizu, H. Tanaka, N. Kanenko, R. Maran, T. Yamada, Y. Imai, O. Sakata, N. Valanoor, and H. Funakubo, *In-situ* observation of ultrafast 90° domain switching under application of an electric field in (100)/(001)-oriented tetragonal epitaxial $\text{Pb}(\text{Zr}_{0.4}\text{Ti}_{0.6})\text{O}_3$ thin films, *Sci. Rep.* **7**, 9641 (2017).
- [33] C. Kwamen, M. Rössle, M. Reinhardt, W. Leitenberger, F. Zamponi, M. Alexe, and M. Bargheer, Simultaneous dynamic characterization of charge and structural motion during ferroelectric switching, *Phys. Rev. B* **96**, 134105 (2017).
- [34] S. Lisenkov, Y. Yao, N. Bassiri-Gharb, and I. Ponomareva, Prediction of high-strain polar phases in antiferroelectric PbZrO_3 from a multiscale approach, *Phys. Rev. B* **102**, 104101 (2020).
- [35] Z. G. Fthenakis and I. Ponomareva, Intrinsic dynamics of the electric-field-induced phase switching in antiferroelectric PbZrO_3 ultrathin films, *Phys. Rev. B* **98**, 054107 (2018).
- [36] J. Baker, M. Paściak, J. Shenton, P. Vales-Castro, B. Xu, J. Hlinka, P. Márton, R. Burkovsky, G. Catalan, A. Glazer, and D. R. Bowler, A re-examination of antiferroelectric PbZrO_3 and PbHfO_3 : an 80-atom *Pnam* structure, [arXiv:2102.08856](https://arxiv.org/abs/2102.08856).
- [37] H. Aramberri, C. Cazorla, M. Stengel, and J. Íñiguez, On the possibility that PbZrO_3 not be antiferroelectric, *npj Comput. Mater.* **7**, 196 (2021).
- [38] B. Xu, O. Hellman, and L. Bellaiche, Order-disorder transition in the prototypical antiferroelectric PbZrO_3 , *Phys. Rev. B* **100**, 020102(R) (2019).
- [39] T. Ma, Z. Fan, B. Xu, T.-H. Kim, P. Lu, L. Bellaiche, M. J. Kramer, X. Tan, and L. Zhou, Uncompensated Polarization in Incommensurate Modulations of Perovskite Antiferroelectrics, *Phys. Rev. Lett.* **123**, 217602 (2019).
- [40] B. K. Mani, C.-M. Chang, S. Lisenkov, and I. Ponomareva, Critical Thickness for Antiferroelectricity in PbZrO_3 , *Phys. Rev. Lett.* **115**, 097601 (2015).

- [41] D. Corker, A. Glazer, J. Dec, K. Roleder, and R. Whatmore, A Re-investigation of the Crystal Structure of the Perovskite PbZrO_3 by X-ray and Neutron Diffraction, *Acta Crystallogr., Sect. B: Struct. Sci.* **53**, 135 (1997).
- [42] Y. Cai, F. Phillipp, A. Zimmermann, L. Zhou, F. Aldinger, and M. Rühle, TEM study of superstructure in a perovskite lead lanthanum zirconate stannate titanate ceramic, *Acta Mater.* **51**, 6429 (2003).
- [43] R. Burkovsky, I. Bronwald, D. Andronikova, B. Wehinger, M. Krisch, J. Jacobs, D. Gambetti, K. Roleder, A. Majchrowski, A. Filimonov, A. I. Rudskoy, S. B. Vakhrushev, and A. K. Tagantsev, Critical scattering and incommensurate phase transition in antiferroelectric PbZrO_3 under pressure, *Sci. Rep.* **7**, 41512 (2017).
- [44] Z. Fu, X. Chen, Z. Li, T. Hu, L. Zhang, P. Lu, S. Zhang, G. Wang, X. Dong, and F. Xu, Unveiling the ferroelectric nature of PbZrO_3 -based antiferroelectric materials, *Nat. Commun.* **11**, 3809 (2020).
- [45] A. Bosak, V. Svitlyk, A. Arakcheeva, R. Burkovsky, V. Diadkin, K. Roleder, and D. Chernyshov, Incommensurate crystal structure of PbHfO_3 , *Acta Crystallogr., Sect. B: Struct. Sci., Cryst. Eng. Mater.* **76**, 7 (2020).
- [46] O. Diéguez, K. M. Rabe, and D. Vanderbilt, First-principles study of epitaxial strain in perovskites, *Phys. Rev. B* **72**, 144101 (2005).
- [47] K. Patel, S. Prosandeev, B. Xu, C. Xu, and L. Bellaiche, Properties of (001) NaNbO_3 films under epitaxial strain: A first-principles study, *Phys. Rev. B* **103**, 094103 (2021).
- [48] V. Y. Topolov, A. Turik, O. Fesenko, and V. Eremkin, Mechanical stresses and three-phase states in perovskite-type ferroelectrics, *Ferroelectr., Lett. Sect.* **20**, 19 (1995).
- [49] N. A. Pertsev and V. G. Koukhar, Polarization Instability in Polydomain Ferroelectric Epitaxial Thin Films and the Formation of Heterophase Structures, *Phys. Rev. Lett.* **84**, 3722 (2000).
- [50] G. Lityagin, D. Andronikova, I. A. Bronwald, M. Kniazeva, M. Jankowski, F. Carla, R. Gao, A. Dasgupta, A. Filimonov, and R. Burkovsky, Intermediate phase with orthorhombic symmetry displacement patterns in epitaxial PbZrO_3 thin films at high temperatures, *Ferroelectrics* **533**, 26 (2018).
- [51] G. Lityagin, A. Vakulenko, R. Gao, A. Dasgupta, A. Filimonov, and R. Burkovsky, Broadening of X-ray reflections and inhomogeneous strain distribution in $\text{PbZrO}_3/\text{SrRuO}_3/\text{SrTiO}_3$ epitaxial heterostructures, in *Journal of Physics: Conference Series*, Vol. 1236 (IOP Publishing, Bristol, England, 2019), p. 012018.
- [52] A. Boulle, O. Masson, R. Guinebretière, and A. Dager, A new method for the determination of strain profiles in epitaxial thin films using x-ray diffraction, *J. Appl. Crystallogr.* **36**, 1424 (2003).
- [53] L. Pintelie, I. Vrejoiu, D. Hesse, G. LeRhun, and M. Alexe, Ferroelectric polarization-leakage current relation in high quality epitaxial $\text{Pb}(\text{Zr}, \text{Ti})\text{O}_3$ films, *Phys. Rev. B* **75**, 104103 (2007).
- [54] G. Kresse and D. Joubert, From ultrasoft pseudopotentials to the projector augmented-wave method, *Phys. Rev. B* **59**, 1758 (1999).
- [55] J. P. Perdew, A. Ruzsinszky, G. I. Csonka, O. A. Vydrov, G. E. Scuseria, L. A. Constantin, X. Zhou, and K. Burke, Restoring the Density-Gradient Expansion for Exchange in Solids and Surfaces, *Phys. Rev. Lett.* **100**, 136406 (2008).
- [56] J. Ricote, D. Corker, R. Whatmore, S. Impey, A. Glazer, J. Dec, and K. Roleder, A TEM and neutron diffraction study of the local structure in the rhombohedral phase of lead zirconate titanate, *J. Phys.: Condens. Matter* **10**, 1767 (1998).
- [57] A. M. Glazer, The classification of tilted octahedra in perovskites, *Acta Crystallogr., Sect. B: Struct. Crystallogr. Cryst. Chem.* **28**, 3384 (1972).
- [58] Analysis of the effects of homogeneous strain on these structures is verbose and will be published separately.
- [59] J. Speck and W. Pompe, Domain configurations due to multiple misfit relaxation mechanisms in epitaxial ferroelectric thin films. I. Theory, *J. Appl. Phys.* **76**, 466 (1994).
- [60] G. Catalan, B. Noheda, J. McAneney, L. J. Sinnamon, and J. M. Gregg, Strain gradients in epitaxial ferroelectrics, *Phys. Rev. B* **72**, 020102(R) (2005).
- [61] S. Alpaly, I. Misirlioglu, V. Nagarajan, and R. Ramesh, Can interface dislocations degrade ferroelectric properties? *Appl. Phys. Lett.* **85**, 2044 (2004).
- [62] A. L. Roytburd, Elastic domains in ferroelectric epitaxial films, in *Thin Film Ferroelectric Materials and Devices* (Springer, New York, 1997), pp. 71–90.
- [63] C. Tan, J. Ouyang, X. Zhong, J. Wang, M. Liao, L. Gong, C. Ren, G. Zhong, S. Zheng, H. Guo, and Y. Zhou, Crystallographically engineered hierarchical polydomain nanostructures in perovskite ferroelectric films, *Acta Mater.* **171**, 282 (2019).
- [64] P. Bak and J. von Boehm, Ising model with solitons, phasons, and the devil's staircase, *Phys. Rev. B* **21**, 5297 (1980).
- [65] A. Artemev, J. Slutsker, and A. Roytburd, Phase field modeling of self-assembling nanostructures in constrained films, *Acta Mater.* **53**, 3425 (2005).
- [66] L.-Q. Chen, Phase-field method of phase transitions/domain structures in ferroelectric thin films: a review, *J. Am. Ceram. Soc.* **91**, 1835 (2008).
- [67] H. Lu, S. Glinsek, P. Buragohain, E. Defay, J. Iñiguez, and A. Gruverman, Probing antiferroelectric-ferroelectric phase transitions in PbZrO_3 capacitors by piezoresponse force microscopy, *Adv. Funct. Mater.* **30**, 2003622 (2020).
- [68] J. He, A. Borisevich, S. V. Kalinin, S. J. Pennycook, and S. T. Pantelides, Control of Octahedral Tilts and Magnetic Properties of Perovskite Oxide Heterostructures by Substrate Symmetry, *Phys. Rev. Lett.* **105**, 227203 (2010).
- [69] J. M. Rondinelli, S. J. May, and J. W. Freeland, Control of octahedral connectivity in perovskite oxide heterostructures: An emerging route to multifunctional materials discovery, *MRS Bull.* **37**, 261 (2012).